frontiers | Frontiers in Earth Science

TYPE Original Research
PUBLISHED 02 March 2023
DOI 10.3389/feart.2023.1135905

OPEN ACCESS

EDITED BY
Xinmin Ge,
China University of Petroleum (East China), China

REVIEWED BY
Zhu Zhaoqun,
Hebei University of Engineering, China
Jingshou Liu,
China University of Geosciences Wuhan, China
Zhongxiang Zhao,
Yangtze University, China

*CORRESPONDENCE
Cunfei Ma,
mcf-625@163.com

SPECIALTY SECTION
This article was submitted to Solid Earth Geophysics, a section of the journal Frontiers in Earth Science

RECEIVED 02 January 2023
ACCEPTED 16 February 2023
PUBLISHED 02 March 2023

CITATION
Huang Z, Yang H, Ye T, Deng H, Guo J, Liang S, Xiao S and Ma C (2023), Characteristics and formation mechanism of Carbonate buried hill fractured-dissolved reservoirs in Bohai Sea, Bohai Bay basin, China. *Front. Earth Sci.* 11:1135905. doi: 10.3389/feart.2023.1135905

Characteristics and formation mechanism of Carbonate buried hill fractured-dissolved reservoirs in Bohai Sea, Bohai Bay basin, China

Zhi Huang[1], Haifeng Yang[1], Tao Ye[1], Hui Deng[1], Jingzhen Guo[1], Shuyi Liang[1], Shuguang Xiao[1] and Cunfei Ma[2]*

[1]Tianjin Branch of CNOOC (China) Co., Ltd., Tianjin, China, [2]School of Geosciences, China University of Petroleum (East China), Qingdao, Shandong, China

Carbonate buried hill madeexploration breakthroughs recently in the offshore Bohai Bay Basin, China, but the plane distribution of the buried hill reservoirs are unclear due to the highly heterogeneous. Taking the CFD2 oilfield as an example, based on core, thin section, seismic, and well logging data, the characteristics of Carbonate buried hill reservoirs in the study area were clarified, the formation mechanism of the reservoirs was discussed, and the development model of the reservoir was established. The results show that the reservoirs are mainly fractured-dissolved reservoirs, and the formation of the reservoirs is mainly related to structural fractures and fluid dissolution along the fractures. The NWW-trending structural fractures were formed under the control of the Indosinian compression, and the NEE-trending structural fractures were formed under the control of the Yanshanian strike-slip transpression. Dolomite is more brittle than limestone and is the main lithology for forming effective fractures. Structural fractures provide favorable channels for atmospheric water dissolution. The C and O isotope values reveal that at least two stages of dissolution have occurred in the study area which are supergene karstification and burial karstification. A model of the fractured-dissolved reservoir under the control of "structure-lithology-fluid" was established. This model highlights that the structural fractures formed by tectonic activities are crucial to reservoir development, and lithology is the internal factor controlling reservoir distribution. Dolomite exhibits the compressive strength of only half of the limestone, and it is the dominant lithology for reservoir development. The dissolution of atmospheric water in the two stages along the fractures greatly improved the physical properties of the reservoirs, and it is the guarantee for the development of effective reservoirs.

KEYWORDS

Carbonate buried hill, structural fracture, fluid dissolution, reservoir development model, Bohai Sea

1 Introduction

Carbonate is an important lithology for hydrocarbon accumulation. Globally, nearly 50% of oil reserves and 25% of gas reserves are endowed in carbonate reservoirs (Li et al., 2016; Ye et al., 2022a). Previous studies have confirmed that karstification is an important factor in controlling the development of carbonate reservoirs. Currently, a variety of development models of karst reservoirs have been established, such as the karst model, quasi-contemporaneous karst model, and fault-karst reservoir development model (Gabrovsek et al., 2004; Zhao W. Z. et al., 2012; Xie et al., 2013; Dong et al., 2021; Guo et al., 2021). These models have guided the exploration discoveries of many large–medium oil and gas fields.

Carbonate buried hill is an important exploration domain in rift basins in eastern China, and it has been widely concerned by petroleum geologists for a long time (Xiao et al., 2018; Hua et al., 2020). Many scholars have worked a lot on Carbonate buried hill reservoirs and realized that these reservoirs correspond to diverse storage spaces and many controlling factors, including lithology, lithofacies, tectonic activity, hydrothermal fluid, and weathering, which also induce complex reservoir-forming mechanisms and distribution models of Carbonate buried hills (Yu et al., 2015; Li et al., 2016; Wang et al., 2016; Ye et al., 2020; Liu C. F. et al., 2022). Therefore, it is of great significance to clarify the characteristics of Carbonate buried hill reservoirs, define the formation mechanism of reservoirs, and establish reservoir development models that conform to geological conditions for the exploration and development of oil fields.

The Bohai Bay Basin on the North China Craton in eastern China is a typical Cenozoic rift basin. The North China Craton was covered in the extensive epicontinental sea during the Paleozoic period, with > 1,000 m thick marine carbonate rocks deposited (Ye et al., 2022b). These carbonate strata formed abundant buried hill traps during the Mesozoic–Cenozoic tectonic activities, which are important oil and gas exploration domains in the Bohai Bay Basin. Since the first discovery of the Lower Paleozoic Carbonate buried hill in Yihezhuang of the Jiyang Depression (Wang and Li, 2017), the Renqiu buried hill and Qianmiqiao buried hill have been confirmed successively, proving the great exploration potential in the Lower Paleozoic in the Bohai Bay Basin (Jin et al., 2001; Zhao X. Z. et al., 2012; Dong et al., 2015; Ma et al., 2020). As a key factor to control hydrocarbon accumulation, the reservoir has always been the focus of research on Carbonate buried hill (Ni et al., 2010; Tang et al., 2013; Zhao et al., 2013; Zhang et al., 2014).

In the offshore Bohai Sea, the most active tectonic area in the Bohai Bay Basin, the Lower Paleozoic reservoirs develop many types and multi-scales of natural fractures as a result of multiple tectonic movements and diagenetic processes in the geological period (Li et al., 2023). The existence of fractures is crucial to reservoir development and hydrocarbon enrichment in the Lower Paleozoic (Ye et al., 2022a). In addition, the later dissolution of multi-source fluids along the fractures greatly improved the physical properties of the reservoirs, forming extensive fractured-dissolved reservoirs (Hua et al., 2020). However, the formation mechanism of structural fractures and the later superimposed dissolution mechanism of diagenetic fluids in the complex superimposed basin of the Bohai Sea are still unknown, which seriously restricts the prediction of fractured-dissolved reservoirs.

In this paper, the Lower Paleozoic buried hill reservoirs in the northwest structural belt of the Shaleitian rise in the Bohai Sea were characterized using the drilling, well logging, core and seismic data, combined with thin section observation and C and O isotope analysis. Specifically, the formation mechanism of fractures and the source of diagenetic fluids were discussed, and the reservoir development model was established finally. The established development model of the fractured-dissolved reservoir is the improvement of the simple karst model, and it can be referential for understanding the development of carbonate reservoirs in regions with strong tectonic activity.

2 Geological setting

The Bohai Bay Basin is a typical Mesozoic–Cenozoic continental rift basin, with an exploration area of about 20×10^4 km^2. The study area underwent a strong transformation of Indosinian and Yanshanian movements in the pre-Cenozoic period, forming abundant NWW- and NEE-trending basement faults (Xu et al., 2019; Ye et al., 2022b). These basement faults were activated in the Cenozoic period and further controlled the Cenozoic basin framework. The Bohai Sea in the central-east part of the basin includes 14 sags and 13 rises, which are alternating in the region. There developed many faults in the Cenozoic basin, and those faults controlled the formation and evolution of the basin and hydrocarbon distribution (Zhou et al., 2010). In the Cenozoic, the Bohai Sea mainly experienced the Paleocene–Eocene rifting, the Oligocene fault depression, and the Miocene–Pliocene depression (Tang et al., 2008; Zhang et al., 2017).

The northwest structural belt of the Shaleitian rise is located in the western part of the Bohai Sea, on the northwest slope of the Shaleitian rise, and adjacent to the Nanpu and Qikou hydrocarbon-rich sags (Figure 1A). With 2×10^3 km^2, the structures mainly trend in near NWW direction, and are modified by near NNE strike-slip fault system. The CFD2 Carbonate buried hill oilfield is an anticline structure formed by reverse faults on the slope belt and contains oil and gas mainly in the Lower Paleozoic strata (Figures 1B, C).

Vertically, from south to north, in the northwest structural belt of the Shaleitian rise, the Archean, Lower Paleozoic, and Mesozoic strata are exposed. The Archaean is dominated by migmatitic granite and granite gneiss. The Cambrian of the Lower Paleozoic is composed of interbedding marine carbonate and mudstone, mainly thick mudstone intercalated with thin dolomite or limestone. The Ordovician of the Lower Paleozoic is a marine carbonate deposit, mainly massive limestone, and dolomite intercalated with thin marl layers. The Mesozoic has the most complex lithology, which is a set of continental clastic rocks containing volcanic rocks, only developed in the low-lying area of the Nanpu sag. The

10.3389/feart.2023.1135905

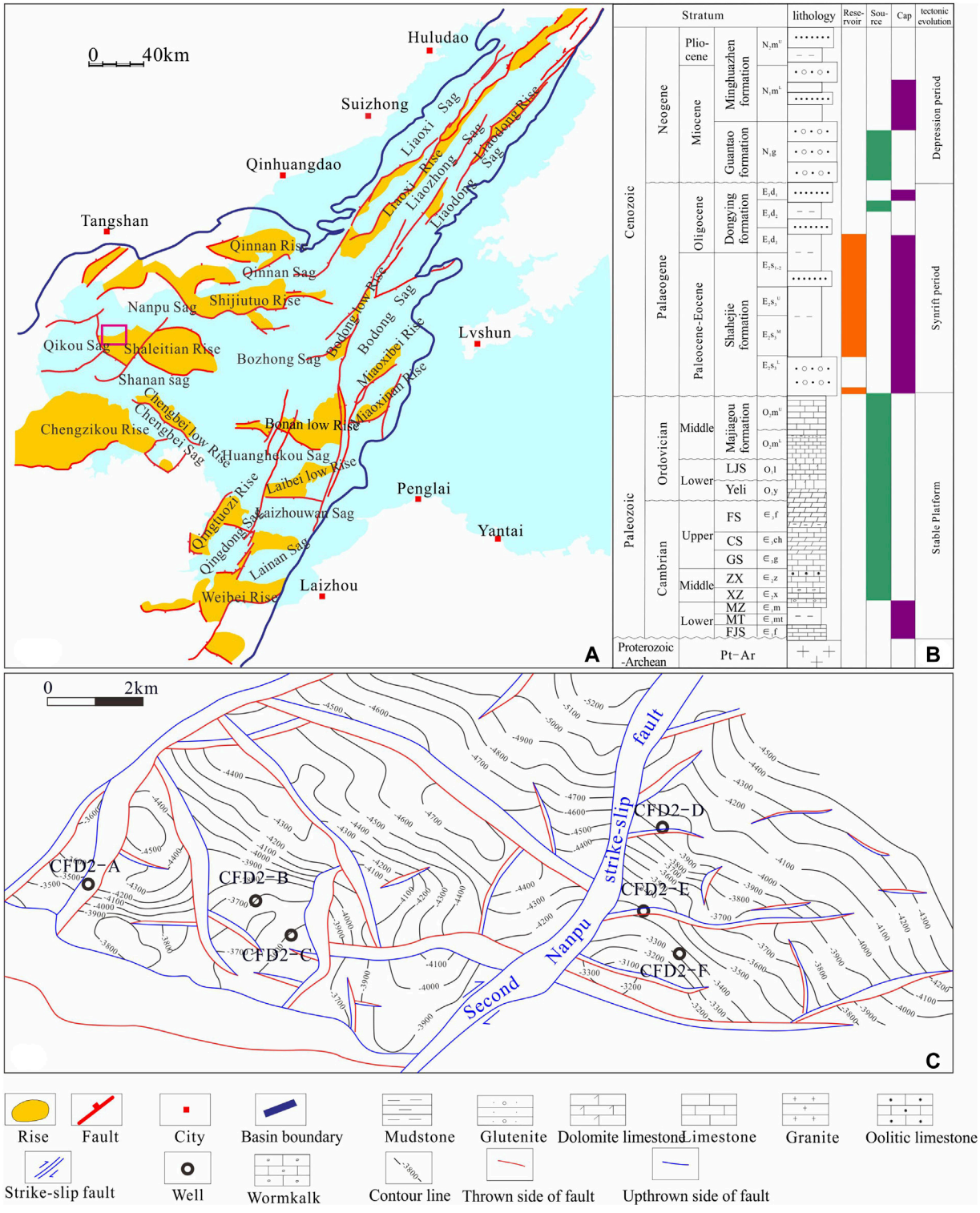

FIGURE 1
(A): Outline Map of the offshore Bohai Bay basin; **(B)** Comprehensive stratigraphic map of the offshore Bohai Bay basin; **(C)** Structural outline map of the CFD2 Oilfield.

overlying Cenozoic develops the Shahejie Formation, Dongying Formation, and Guantao Formation-Pingyuan Formation, from bottom to top. Moreover, the Cenozoic strata gradually overlap and become younger from north to south, and only the Guantao Formation and the Minghuazhen Formation are developed at the high of the rise (Wang et al., 2016; Huang et al., 2017).

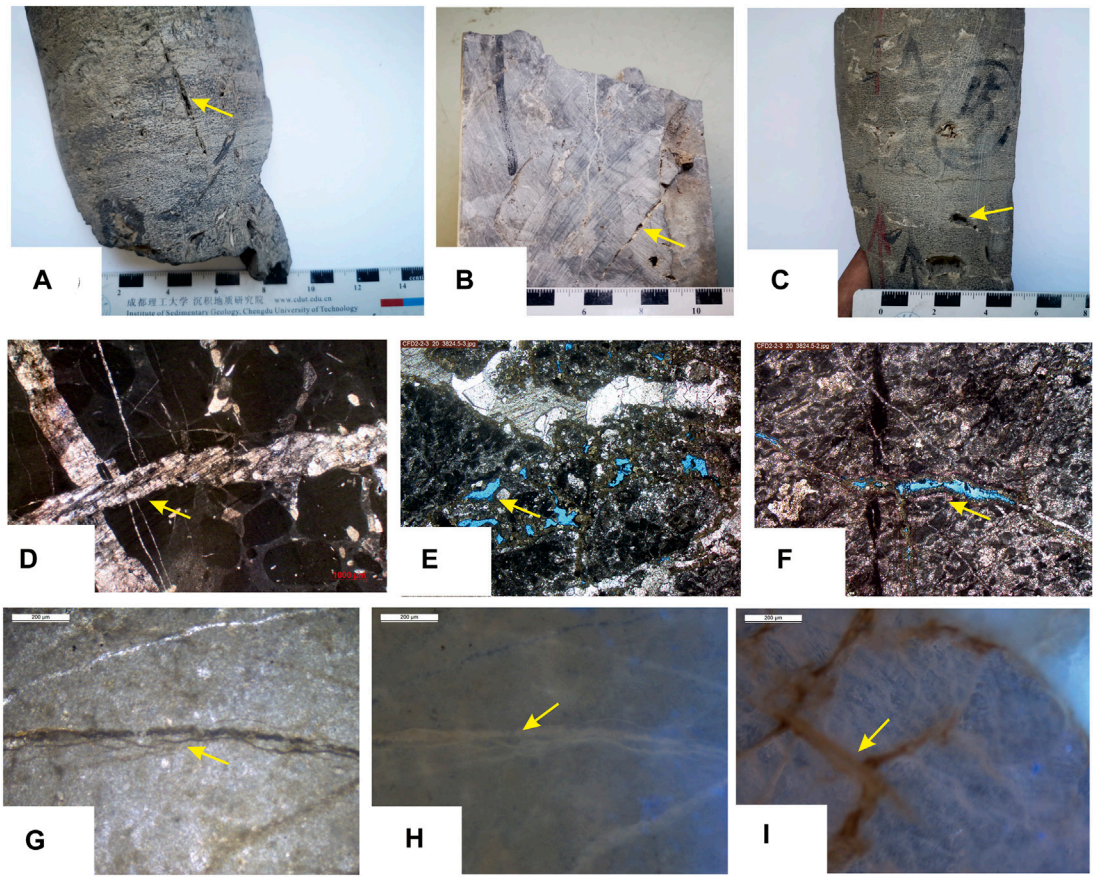

FIGURE 2
(A): Fractures in cores; **(B)** Fractures with dissolved pore in cores; **(C)** Fractures with dissolved holes in cores; **(D)** Fractures in thin section, noting the cutting of two set of fractures; **(E)** Fractures in thin section, noting the corrosion along fractures; **(F)** Fractures in thin section, noting the corrosion in fractures; **(G)** Fractures in thin section, Asphalt filling inside fractures; **(H)** Fractures in thin section, noting the fluorescence in the fracture, which indicating that the fracture is an important migration channel; **(I)** Network fractures in thin sections filled with oil.

3 Data and method

The samples in this study were taken from the exploration wells (e.g., CFD2-A, CFD2-B, CFD2-C, CFD2-D, CFD2-E, and CFD2-F) in the Lower Paleozoic Carbonate buried hill in the Shaleitian rise. The data include drilling core data, sidewall coring data, 3D seismic data, conventional well logging curves, and imaging logging curves. In order to characterize the fractures, we observed 73 m drilling cores and described 214 sidewall cores of 6 wells. We prepared thin sections and observed cast for each sidewall cores to identify the main types of storage space in the reservoirs. We also observed fluorescence on key thin sections to determine hydrocarbon-bearing properties and the effectiveness of fractures. We analyzed the electric imaging logging data of each exploration well to determine the strike and dip angle of the effective fractures. In order to determine the geological factors controlling the formation of fractures, we used the geological profile interpreted by seismic data to restore the evolution process of buried hills. Based on the analysis of regional tectonic evolution, we analyzed the main fracture initiation events and their role in forming fractures. The carbon and oxygen isotopes of these samples were measured using a mass spectrometer (2019.FLS0167/SN09609D) in the Experimental Center of China National Offshore Oil Corporation (Ye et al., 2022a). In combination with the C and O isotope measurements of fracture fillings, we discussed the source of diagenetic fluids. In addition, we measured the physical properties of 105 typical samples, so that we can quantitatively determine the development of the reservoirs. In order to reveal the control effect of tectonic activity and fracture distribution, based on the structural map of the top of the buried hill, the maximum stress of the stratum was obtained by finite element simulation.

4 Results

4.1 Reservoirs

The analysis of drilling cores, sidewall cores, and fluorescence thin sections reveal that there are several types

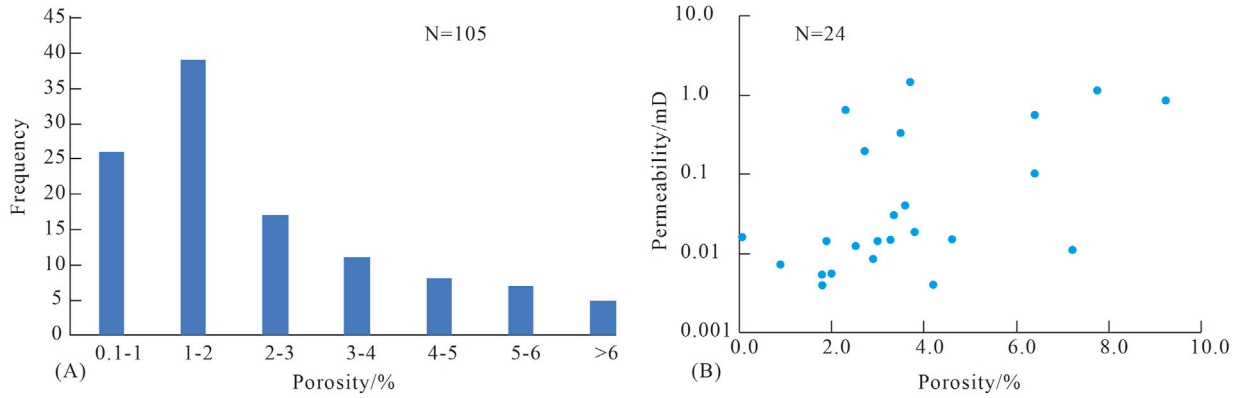

FIGURE 3
Physical properties of Carbonate buried hill reservoirs in CFD area [**(A)**: Porosity distribution; **(B)** Porosity-permeability correlation].

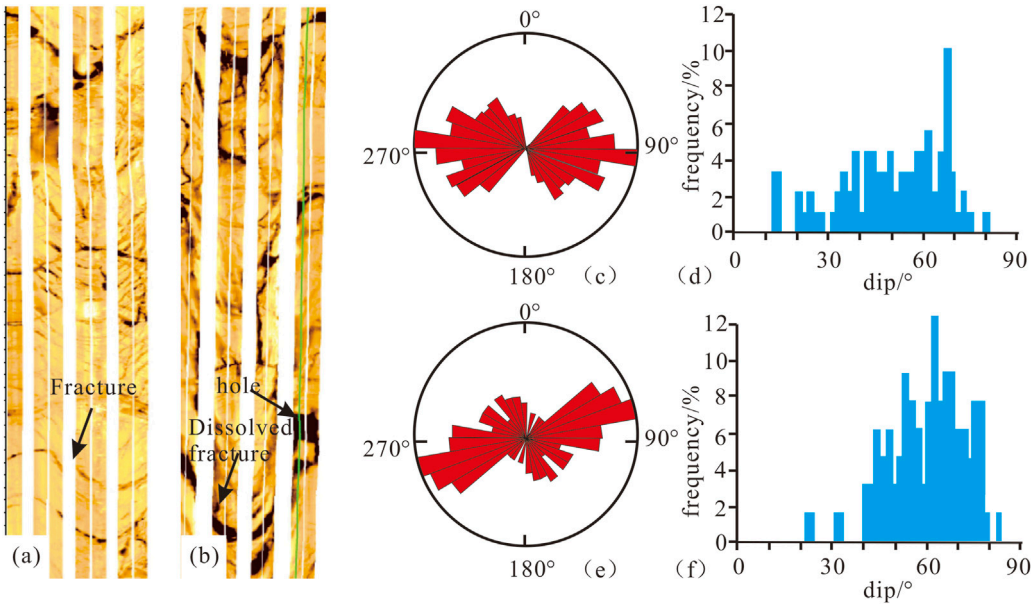

FIGURE 4
Fracture development in Carbonate buried hill reservoirs in the CFD2 area. [**(A)**: Imaging logging response of structural fractures; **(B)** Imaging logging response of dissolved fractures; **(C,D)** Trend and dip angle of structural fractures in Well CFD2-B; **(E,F)** Trend and dip angle of structural fractures in Well CFD2-A].

of reservoirs in the study area, including fractured, fractured-dissolved, and dissolved pore/vug reservoirs, with the fractured-dissolved reservoirs in dominance. A large number of fractures can be observed on the drilling cores. The fractures have straight surfaces, indicating that they are mainly structural fractures. The statistics of drilling cores show that fracture opening varies greatly, in a range of 0.5–8 mm. There are abundant dissolved pores/vugs along the fractures, with maximum diameter of 1.3–12 mm. Note that the dissolved pores/vugs are mainly distributed along the structural fractures (Figures 2A–C).

Numerous structural fractures can be seen on the thin section, with the characteristics of mutual cutting, indicating at least two stages of fracture initiation events (Figure 2D). Microscopically, many fractures are obverse to have been filled with calcite in the late stage (Figure 2D). The fillings are obviously different, and can be divided into silty-fine crystal filling and coarse crystal filling. There are also many unfilled

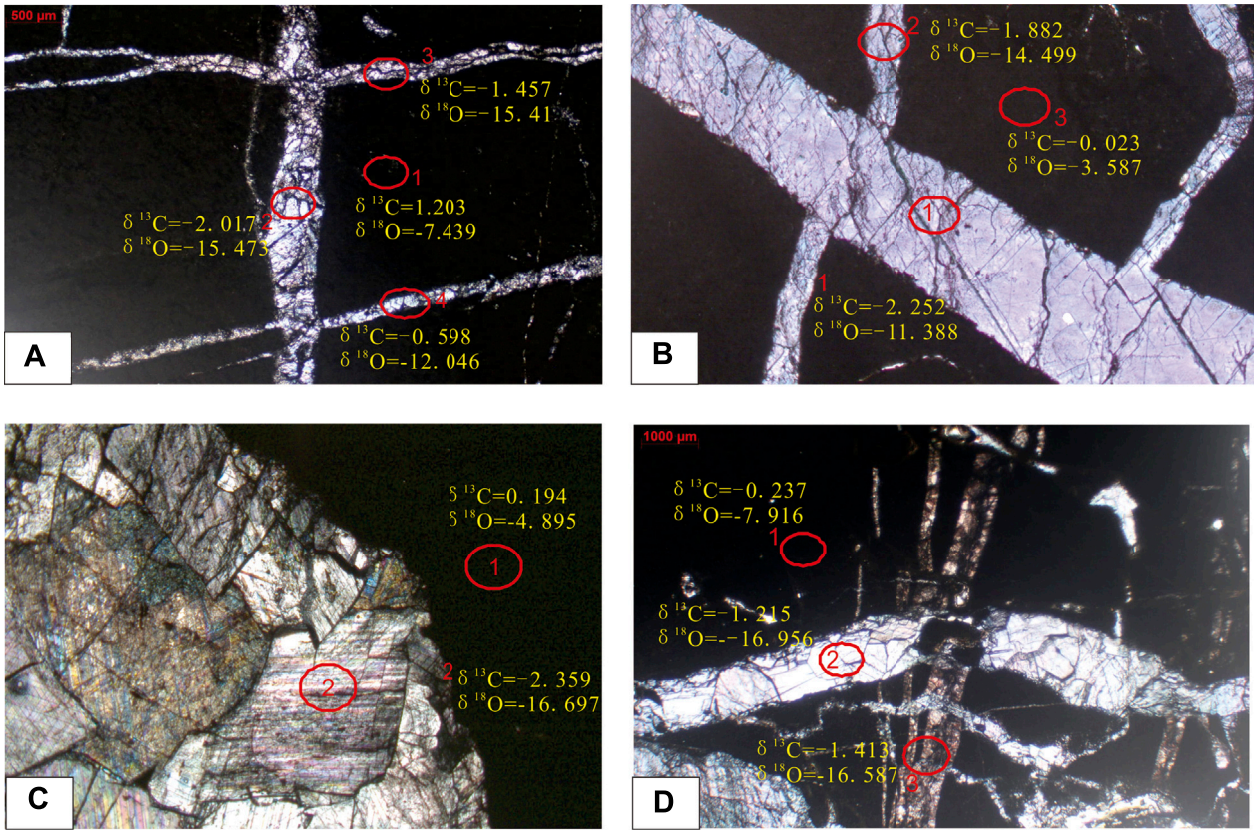

FIGURE 5
Fillings in structural fractures in buried hill and their C and O isotopes. [**(A)**: 3563.18 m; **(B)** 3563.43 m; **(C)** 3565.15 m; **(D)** 3565.53 m, as shown in Table 1].

fractures, along which strong dissolution characteristics can be seen, which is consistent with the observation results of drilling cores (Figures 2E, F). Asphalt can be seen in the fractures in the thin section (Figure 2G). In the fluorescence thin section, abundant oil and gas shows can be seen, which indicates that both structural fractures and dissolved pores in the study area are the main effective storage spaces (Figures 2H, I).

The physical properties of 105 sidewall cores were measured. The porosity is 0.1%–9.3%, concentrated at 1%–3%, and a lot of samples exhibit the porosity ˂ 5% (Figure 3A). The permeability is mainly ˂ 10 mD, and a lot of many samples exhibit the permeability of 0.01–1 mD. The cross plot shows that the porosity and the permeability are less correlated (correlation coefficient was 0.2208), indicating that the reservoir is mainly a fractured-porous medium (Figure 3B), which is consistent with the observation results of drilling cores and thin sections.

4.2 Fractures

Structural fractures are extremely developed in the study area. Numerous structural fractures are observed on cores and thin sections. The occurrence and dip angle of the structural fractures were depicted by electric imaging logging. It is found that there are mainly two groups of fractures in the CFD area: NEE, and NWW, by tending, with the NEE-trending fractures in dominance. The structural fractures show an obvious sine dark curve on the electric imaging log, and medium-sized pores/vugs can be seen along the structural fractures. In addition, some fractures are relatively wide and may be dissolved by atmospheric water (Figures 4A, B). The fractures are quite different in dip angle: the NWW-trending fractures have the dip angles of 30°–80°, with an average of 48°; the NEE-trending fractures have the dip angles of 50°–80°, with an average of 67°. Clearly, the NEE-trending fractures show higher dip angles than the NWW-trending fractures, possibly suggesting that they were formed in different tectonic settings (Figures 4C–F).

4.3 Fracture fillings

Fracture fillings are important for revealing diagenetic fluids. There are a huge amount of calcite fillings in the structural fractures in the study area. The C and O isotopes of fillings in fractures and surrounding rocks were analyzed to determine the source of diagenetic fluids. It is found that the C isotope of surrounding rocks is generally positive and

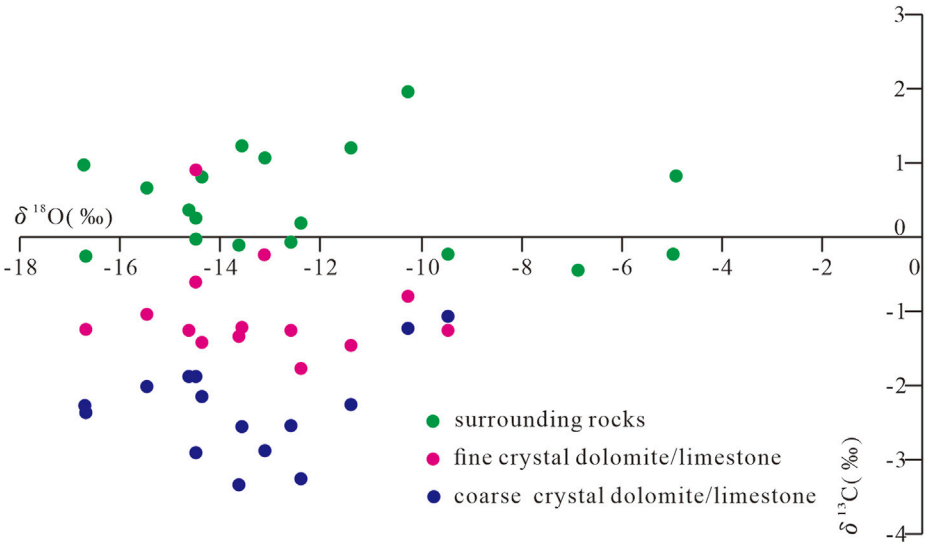

FIGURE 6
Cross-plot of C and O isotopes of surrounding rocks and structural fracture fillings in the buried hill.

occasionally negative, mostly greater than −1‰, and the O isotope is between −18‰ and −4‰, representing the isotopic characteristics of seawater during sedimentation.

The fracture fillings exhibit significantly different C and O isotopes from the surrounding rocks. According to the crystallization degree, they can be divided into silty-fine crystal dolomite and limestone, and coarse crystal dolomite and limestone, which are different in the C and O isotopes. For the silty-fine crystal dolomite and limestone, the C isotope ranges from −2‰ to 0‰, and the O isotope from −18‰ to −8‰. For the coarse crystal dolomite and limestone, the C isotope ranges from −4‰ to −2‰, and the O isotope from −18‰ to −8‰. It can be seen that the coarse crystal fillings are equivalent to the fine crystal fillings in the O isotope, but display a lower C isotope generally, possibly indicative of different diagenetic environments (Figures 5, 6; Table 1).

5 Discussion

5.1 Formation mechanism and distribution of fractures

The formation and distribution of structural fractures are often related to strong tectonic activities (Ye et al., 2022b; Guo et al., 2022). In the study area, the fractures were mainly formed due to the Indosinian and Yanshanian tectonic activities, with the former inducing NWW-trending fractures and the latter inducing NEE-trending fractures (Figure 4).

Based on the geological profile, the tectonic evolution process of the CFD area was restored. This area deposited a set of epicontinental sea carbonate during the early Paleozoic and a set of transitional deposits during the late Paleozoic (Figure 7A). The collision between the South China Plate and the North China Plate in the Indosinian induced a series of NWW-trending thrust faults in the study area, and also caused the Paleozoic fold deformation (Figure 7B). The NWW-trending faults stopped their activity in the Yanshanian (Figure 7C). At this time, a group of NEE-trending strike-slip faults was formed, and they were mainly featured by sinistral compression, leading to the uplift and fold deformation of the strata near the fault belt (Figure 8). Since the Himalayan, the NWW-trending faults had been reactivated and controlled the deposition of Paleogene, and the buried hill was finally buried and shaped (Figures 7D, E).

The multi-phase tectonic activities in the buried hill provided favorable external stress for the development of structural fractures. During the Indosinian compression, the CFD area was close to the thrust fault belt, and a large number of NWW-trending fractures were developed near the NWW fault belt. For example, the imaging logging data of Well CFD2-F and Well CFD2-C reveal that the NWW-trending fractures have low dip angles, possibly because they were formed in the thrust nappe setting.

During the formation of the strike-slip fault, intense fracturing deformation might occur along the fault belt, thus deriving a great number of structural fractures (Zhang et al., 2010; Liu J. S. et al., 2022; Yun and Deng, 2022). However, the distribution of fractures controlled by strike-slip faults is complex, which is related to the specific spatial shape of faults and the derived local stress field. Strike-slip faults present differences role in the distribution of fractures, in which the stress in the strong deformation zone of the strata near the strike-slip fault zone is the most concentrated and is the main development zone of fractures. The structural fractures

10.3389/feart.2023.1135905

TABLE 1 Characteristics of C and O isotopes of surrounding rocks and fracture fillings in the CFD area.

Well	Depth (m)	Sample type	Lithology	δ^{13}CPDB (‰ PDB)	δ^{18}OPDB (‰ PDB)
CFD2-A	3562.1	Surrounding rock	Fine crystal dolomite	−0.258	−4.908
CFD2-A	3562.26	Surrounding rock	Micrite dolomite	1.232	−4.958
CFD2-A	3562.26	Fracture filling	Fine crystal dolomite	−1.242	−9.265
CFD2-A	3562.45	Fracture filling	Coarse crystal limestone	−2.547	−13.574
CFD2-A	3562.45	Surrounding rock	Micrite limestone	0.812	−6.868
CFD2-A	3562.45	Fracture filling	Coarse crystal limestone	−2.152	−14.378
CFD2-A	3562.5	Surrounding rock	Fine crystal dolomite	0.668	−5.587
CFD2-A	3563.18	Surrounding rock	Micrite limestone	1.203	−7.439
CFD2-A	3563.18	Fracture filling	Coarse crystal limestone	−2.017	−15.473
CFD2-A	3563.18	Fracture filling	Fine crystal limestone	−1.457	−15.41
CFD2-A	3563.18	Fracture filling	Fine crystal limestone	−0.598	−12.046
CFD2-A	3563.43	Fracture filling	Coarse crystal limestone	−2.252	−11.388
CFD2-A	3563.43	Fracture filling	Coarse crystal limestone	−1.882	−14.499
CFD2-A	3563.43	Surrounding rock	Micrite dolomite	−0.023	−3.587
CFD2-A	3565.1	Fracture filling	Coarse crystal limestone	−3.263	−12.393
CFD2-A	3565.1	Fracture filling	Coarse crystal limestone	−1.058	−9.465
CFD2-A	3565.1	Fracture filling	Coarse crystal limestone	−1.225	−10.258
CFD2-A	3565.15	Surrounding rock	Micrite dolomite	0.194	−4.895
CFD2-A	3565.15	Fracture filling	Coarse crystal dolomite	−2.359	−16.697
CFD2-A	3565.53	Surrounding rock	Micrite limestone	−0.237	−7.916
CFD2-A	3565.53	Fracture filling	Fine crystal dolomite	−1.215	−16.956
CFD2-A	3565.53	Fracture filling	Fine crystal dolomite	−1.413	−16.587
CFD2-A	3565.61	Fracture filling	Coarse crystal limestone	−3.334	−13.632
CFD2-A	3565.61	Fracture filling	Coarse crystal limestone	−2.543	−12.587
CFD2-A	3565.95	Surrounding rock	Micrite limestone	1.955	−3.758
CFD2-A	3565.95	Fracture filling	Fine crystal dolomite	−1.041	−15.725
CFD2-A	3566.08	Surrounding rock	Micrite dolomite	−0.108	−6.976
CFD2-A	3566.08	Fracture filling	Fine crystal limestone	−1.778	−11.955
CFD2-A	3566.14	Surrounding rock	Micrite dolomite	−0.069	−3.184
CFD2-A	3566.14	Fracture filling	Coarse crystal limestone	−1.884	−14.628
CFD2-A	3566.26	Surrounding rock	Micrite dolomite	0.361	−2.316
CFD2-A	3566.26	Fracture filling	Fine crystal limestone	−1.247	−11.265
CFD2-A	3566.26	Fracture filling	Coarse crystal limestone	−2.914	−14.499
CFD2-A	3566.74	Surrounding rock	Micrite dolomite	0.254	−2.946
CFD2-A	3566.74	Fracture filling	Coarse crystal limestone	−2.887	−13.12
CFD2-A	3566.8	Surrounding rock	Micrite limestone	1.073	−5.779
CFD2-A	3566.8	Fracture filling	Fine crystal limestone	−0.798	−10.833
CFD2-A	3567.09	Fracture filling	Fine crystal limestone	−1.343	−8.234

(Continued on following page)

TABLE 1 (*Continued*) **Characteristics of C and O isotopes of surrounding rocks and fracture fillings in the CFD area.**

Well	Depth (m)	Sample type	Lithology	δ^{13}CPDB (‰ PDB)	δ^{18}OPDB (‰ PDB)
CFD2-A	3567.09	Fracture filling	Fine crystal limestone	−1.258	−11.254
CFD2-A	3567.31	Surrounding rock	Micrite dolomite	0.974	−6.046
CFD2-A	3567.31	Surrounding rock	Micrite dolomite	0.827	−6.82
CFD2-A	3567.6	Surrounding rock	Micrite dolomite	−0.221	−5.382
CFD2-A	3567.6	Fracture filling	Fine crystal limestone	−1.254	−8.547
CFD2-A	3567.6	Fracture filling	Coarse crystal limestone	−2.255	−16.732
CFD2-A	3567.77	Surrounding rock	Micrite limestone	−0.451	−6.689
CFD2-A	3567.77	Fracture filling	Fine crystal limestone	0.909	−7.982
CFD2-A	3567.77	Fracture filling	Fine crystal limestone	−0.238	−7.917

formed by the strike-slip fault belt are mainly located inside the main fault belt, but when the trend of the strike-slip fault belt changes, the local stress field derived from it forms the "sweet spot" of fractures (Yu et al., 2014; Li et al., 2021). Field measurement shows that obvious pressure increases and pressure-releasing belts are formed at the strike-slip bending position. The pressure-increasing belt is often accompanied by terrain uplifting and the creation of numerous structural fractures, while the pressure-releasing belt mostly forms graben with few fractures (Wei, 2015). Abundant NEE-trending fractures were developed near the NEE fault belt during the Yanshanian, especially in the strong uplifting area of the buried hill caused by strike-slip faults, where the fracture density is the largest. For instance, all the fractures in Wells CFD2-D, CFD2-E, CFD2-F, and CFD2-C mainly trend in the NEE direction (Figure 8). It is worth noting that the structural fractures induced by strike-slipping have high dip angles, and they exhibit higher effectiveness than the NWW-trending fractures.

The formation of a high-quality buried hill reservoir is not only affected by external factors but also related to the physical properties of the rock itself (Hou et al., 2015; Wang et al., 2015). The compressive strength of rock determines its ability to form fractures. The lower the compressive strength, the more easily the rock forms fractures (Guo et al., 2018). Compressive strength tests on different lithologies confirm that the compressive strength is 49 MPa for dolomite, 70.74 MPa for limy dolomite, 75.4 MPa for dolomitic limestone, and 104.9 MPa for limestone; that is, with the increase of dolomite content in carbonate, the compressive strength tends to decrease gradually (Figure 9B). It is worth noting that the compressive strength of dolomite is only half of that of limestone, that is, the stress required for dolomite to break and form structural fractures is only half of that of limestone. This means that the higher the content of dolomite, the easier the rock is to break and form structural fractures.

The linear density of fractures in intervals with different dolomite contents was calculated by imaging logging data, element well-logging data, and mud logging data. The results show that, except for a small amount of limestones (low dolomite content) that exhibit high fracture density, the overall fracture density increases significantly with the increase of dolomite content (Figure 9A), which also confirms the control of lithology on fracture distribution in the study area. A lot of drilling data verify that at the structural high near the fault belt, both limestone and dolomite can form high-quality reservoirs, while at the structural low and inside the buried hill, high-quality reservoirs are mainly developed in intervals with high dolomite content. Essentially, in the interior of the buried hill and at the structural low, where the stress is weak, the limestone is difficult to form fractures, while the dolomite with lower compressive strength is broken to become reservoirs.

5.2 Fracture dissolution mechanism and reservoir development model

Structural fractures provide good pathways for fluid flow, which is the basis for the development of karst reservoirs. The negative carbon isotope anomaly is mainly related to the influence of organic carbon; The negative oxygen isotope anomaly is mainly affected by the leaching of hydrothermal solution or atmospheric water. According to the observation of fracture fillings and the analysis results of C and O isotopes, at least two stages of karstification have occurred in the study area. In the first stage, the fillings were mainly silty-fine crystal carbonate, with the C isotope ranging from −2‰ to 0‰ and the O isotope ranging from −16‰ to −8‰, which may represent the atmospheric freshwater dissolution in the supergene period. In the second stage, the fillings were mainly coarse crystal carbonate, with the C isotope ranging from −4‰ to −2‰ and the O isotope ranging from −18‰ to −8‰, indicating that the diagenetic temperature was higher than that in the first stage, which may be related to karstification during burial.

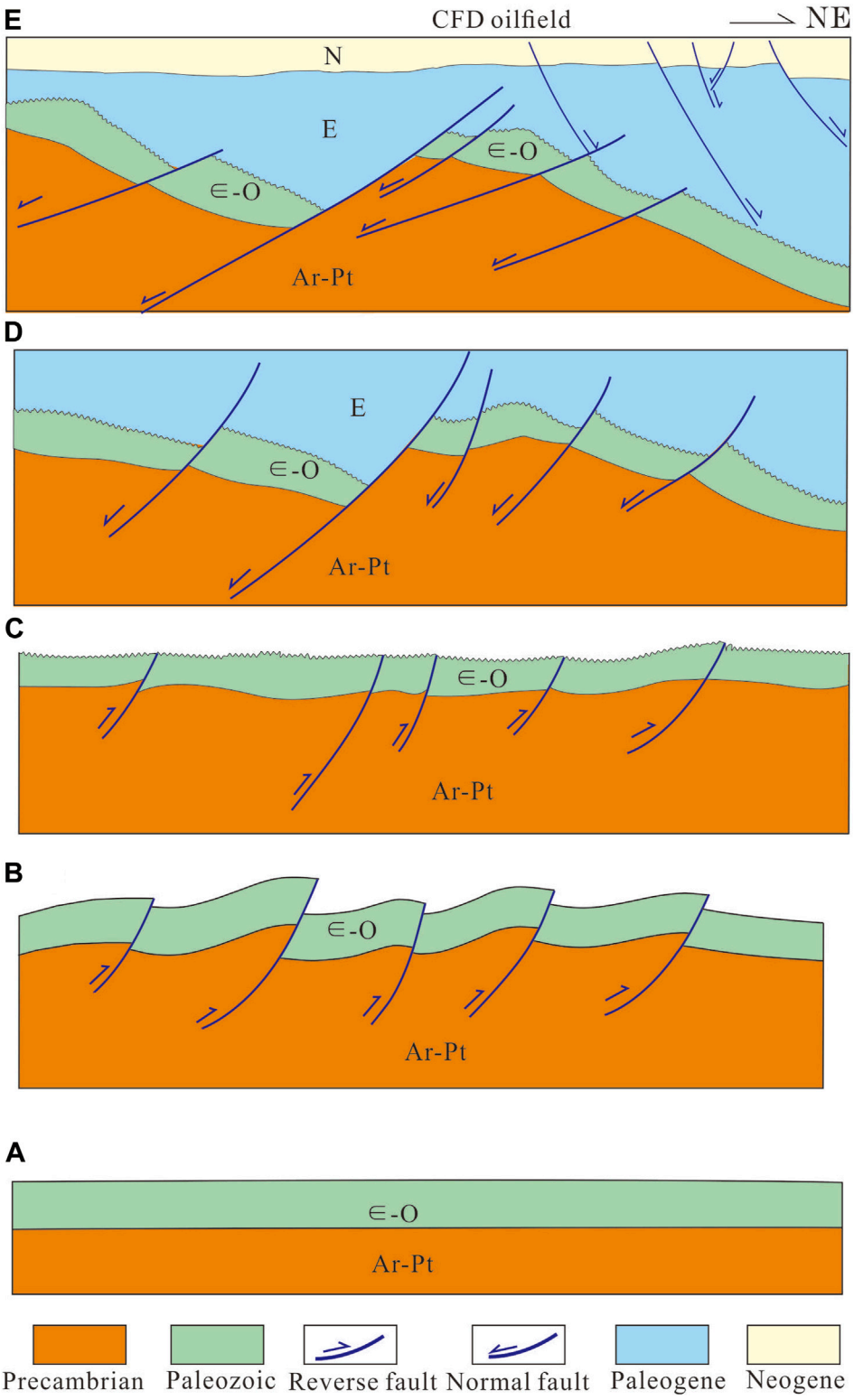

FIGURE 7
(A): The stable tectonic background before the Indosinian movement; **(B)** Development of the thrust-related folds during the Indosinian movement; **(C)** Continuous uplift and denudation during the Yanshan movement; **(D,E)** Buried hills are gradually buried and shaped during the Cenozoic period.

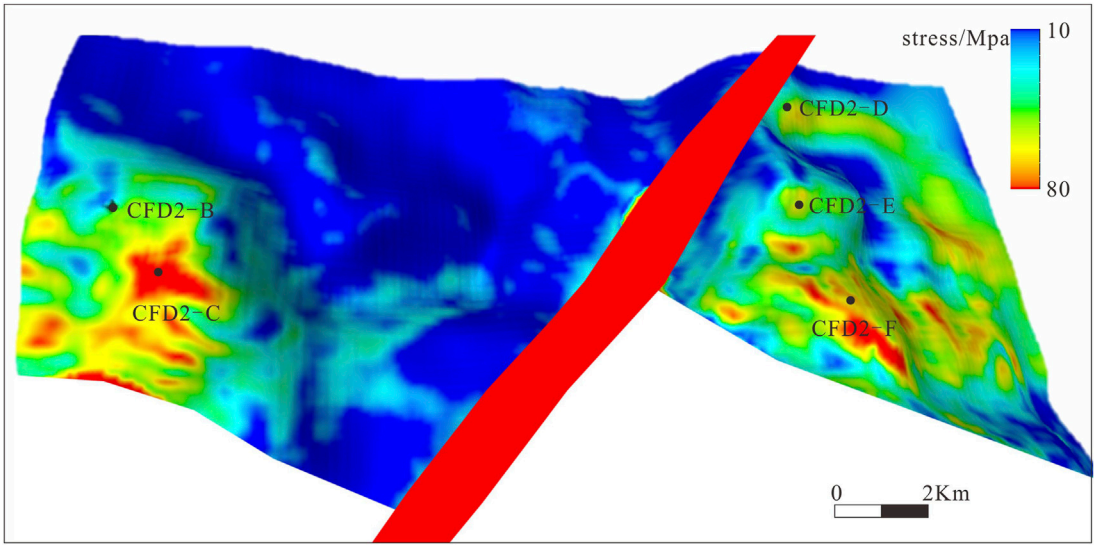

FIGURE 8
Maximum stress concentration by formation deformation induced by sinistral strike-slip activity.

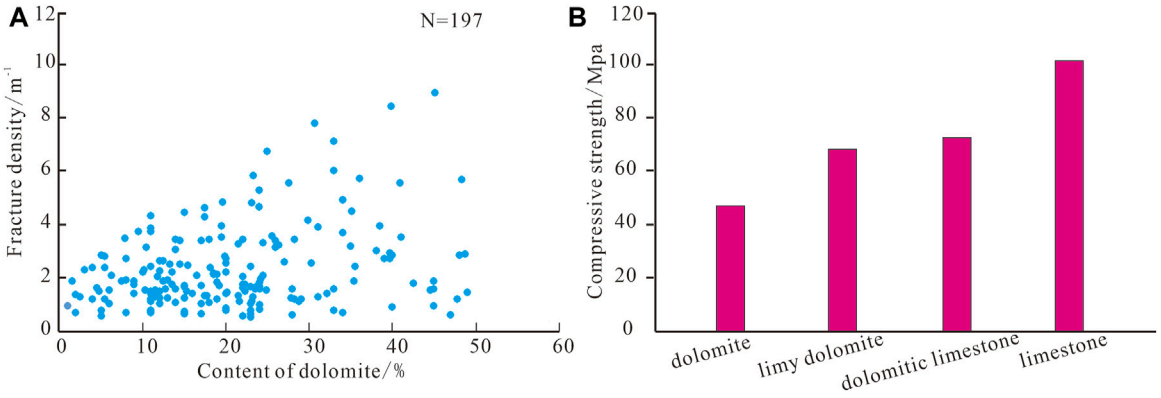

FIGURE 9
Compressive strength and fracture density of different lithologies. [**(A)**: Dolomite content vs. fracture density; **(B)** Compressive strength of different lithologies, after Zhu et al., 2017)].

Combined with the tectonic evolution process and the above analysis, the development model of Carbonate buried hill reservoirs in the CFD area was established. In the study area, fractured-dissolved reservoirs are dominant. The early structural fractures provide flow pathways for later fluid dissolution, which is the key to controlling the development of reservoirs. The distribution of high-quality reservoirs is jointly controlled by structure, lithology, and fluid. Before Indosinian period, the tectonic setting was relatively quietly (Figure 10A). During the Indosinian, nearly NWW folds were formed in the study area due to SN compression, and intensive fracture belts were formed near the Indosinian thrust fault belt. Meanwhile, the first supergene karstification occurred (Figure 10B). Subsequently, the NEE intensive fault belt was formed near the strike-slip faults by the strike-slip transpression process during the Yanshanian. At this time, the Paleozoic buried hill was still exposed and the supergene dissolution continued (Figure 10C). Under this background, the fracture fillings showed a relatively high C isotope. In the Himalayan, due to the continuous extension, the Paleozoic strata experienced burial karstification along bedding on the slope, leading to more negative C isotope of the fillings, due to large burial depth (Figure 10D). With the continuous burial in the Cenozoic, the O isotope became generally negative, and finally the present reservoir pattern was formed (Figures 10E, F).

Based on the above analysis, the development model of fractured-dissolved reservoirs was established. The stress is most concentrated near the Indosinian and Yanshanian faults, which are the dominant areas with fractures developed. Dolomite is more brittle than limestone, and may more easily form structural fractures in the process of structural transformation, thus it is the lithology

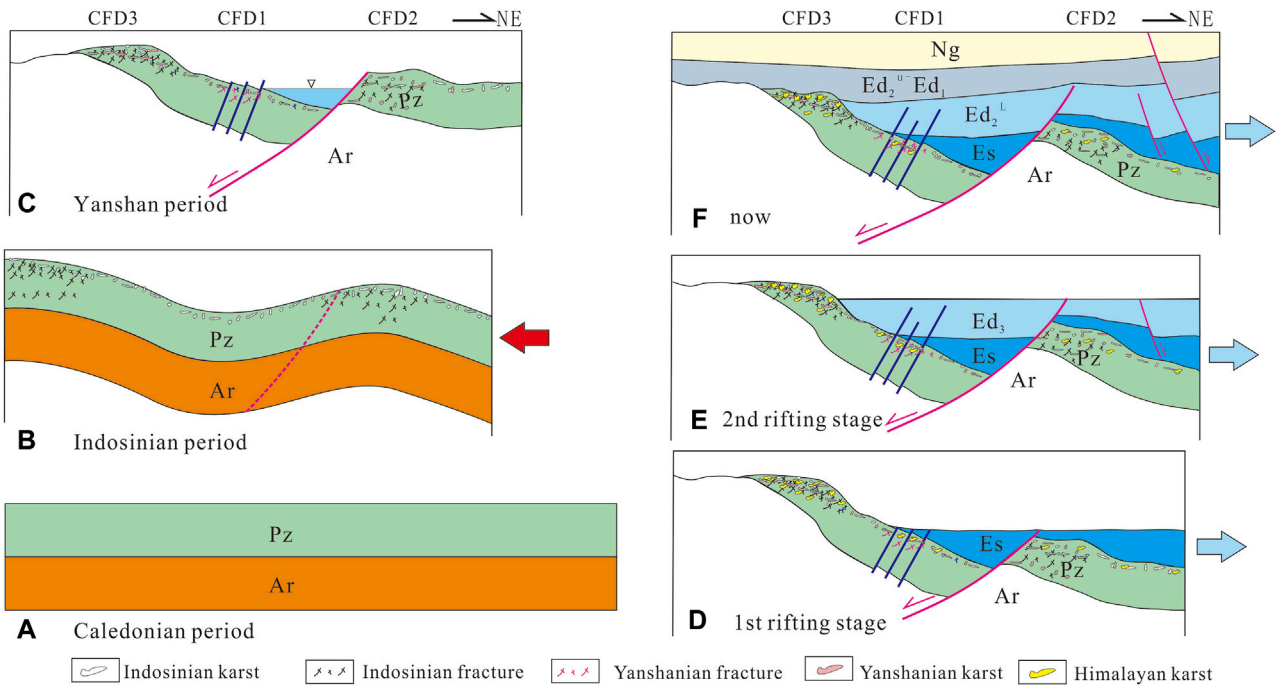

FIGURE 10
(A): The stable tectonic setting during the pre-Indosinian period; **(B)** The fracturing and exposed dissolution during the Indosinian thrust folding process; **(C)** The fracturing and exposed dissolution during the Yanshan strike-slip activity; **(D,E)** Differential burial and dissolution process during the Paleogene ;**(F)** Deep bury during the Neogene.

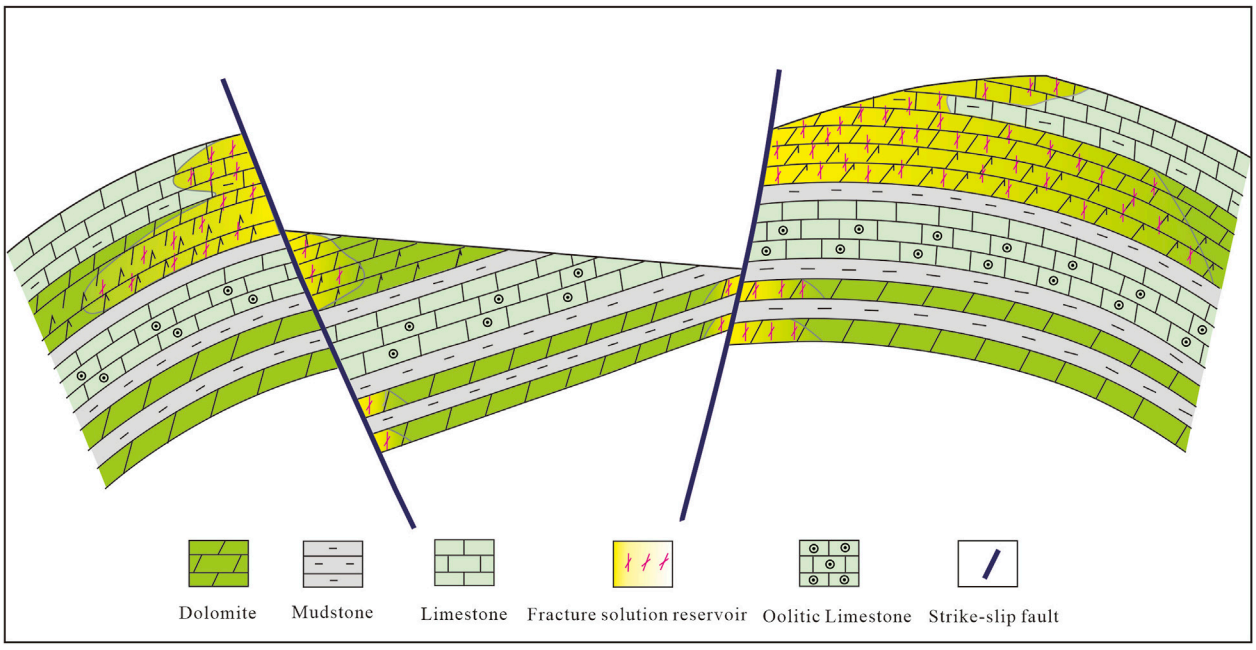

FIGURE 11
Development model of fractured-dissolved reservoirs in CFD area.

favorable for reservoir development. The preexisting structural fractures experienced two types of dissolution with different properties in the supergene stage and the burial stage, which further improved the physical properties of the reservoirs and guaranteed the development of effective high-quality reservoirs (Figure 11).

6 Conclusion

The Carbonate buried hill reservoirs in the CFD area are mainly fractured-dissolved reservoirs. The formation of these reservoirs is mainly related to structural fractures and fluid dissolution along the fractures. There are two groups of structural fractures: NWW and NEE, by trending. The C and O isotopes reveal that the diagenetic fluid is mainly atmospheric fresh water.

The formation of NWW- and NEE-trending structural fractures is respectively controlled by Indosinian compression and Yanshanian strike-slip transpression. Dolomite is more brittle than limestone and is the main lithology for forming effective fractures. The structural fractures provide favorable channels for the dissolution of atmospheric water. The C and O isotopes reveal that at least two stages of dissolution have occurred in the study area: 1) the supergene karstification, when fine-silty crystal carbonate was mainly filled; and 2) the burial karstification, when coarse crystal carbonate was mainly filled.

The development model of fractured-dissolved reservoirs under the control of structure, lithology, and fluid was established. This model emphasizes that structural fractures formed by tectonic activities are the key to reservoir development, and lithology is the internal factor controlling reservoir distribution. Dolomite exhibits compressive strength as only half of the limestone, and it is the dominant lithology for reservoir development. The two phases of dissolution of atmospheric water along the fractures greatly improved the physical properties of the reservoirs, which is the guarantee for the development of effective reservoirs.

Data availability statement

The original contributions presented in the study are included in the article/Supplementary Material, further inquiries can be directed to the corresponding author.

Author contributions

ZH: come up with ideas; HY: project guidance; TY: writing; HD: data processing; JG: drawing figures; SL: data collecting; SX: language check; CM: funding.

Conflict of interest

Authors ZH, HY, TY, HD, JG, SL, and SX were employed by Tianjin Branch of CNOOC (China) Co., Ltd.

The remaining author declares that the research was conducted in the absence of any commercial or financial relationships that could be construed as a potential conflict of interest.

Publisher's note

All claims expressed in this article are solely those of the authors and do not necessarily represent those of their affiliated organizations, or those of the publisher, the editors and the reviewers. Any product that may be evaluated in this article, or claim that may be made by its manufacturer, is not guaranteed or endorsed by the publisher.

References

Dong, Y. H., Duan, R. Q., Li, Z., Lv, X. X., Cai, C. F., Liu, J. Q., et al. (2021). Quantitative evaluation of hydrothermal fluids and their impact on diagenesis of deep carbonate reservoirs: Insights from geochemical modeling. *Mar. . Petroleum. Geol.* 124, 104797. doi:10.1016/j.marpetgeo.2020.104797

Dong, Y. X., Zhao, Z. J., Cao, Z. H., Wang, J. G., Gong, F. X., Wang, P. X., et al. (2015). Exploration potential and significance of Ordovician carbonate karst monadnock traps in Nanpu sag. *Acta pet. sin.* 36 (006), 653–663. doi:10.7623/syxb201506002

Gabrovsek, F., Romanov, D., and Dreybrodt, W. (2004). Early karstification in a dual-fracture aquifer: The role of exchange flow between prominent fractures and a dense net of fissures. *J. hydrology J. Hydrol.* 299, 45–66. doi:10.1016/j.jhydrol.2004.02.005

Guo, R. X., Zhang, S. N., Wang, K., Han, M. M., and Ding, X. Q. (2021). Multiphase dolomitization and hydrothermal alteration of the upper cambrian-lower ordovician carbonates in the gucheng uplift, Tarim basin (NW China). *J. petroleum Sci. Eng. Petrol. Sci. Eng.* 206, 108964. doi:10.1016/j.petrol.2021.108964

Guo, X., Liu, R., Xu, S., Feng, B., Wen, T., and Zhang, T. (2022). Structural deformation of shale pores in the fold-thrust belt: The wufeng-longmaxi shale in the anchang syncline of central Yangtze block. *Adv. Geo-Energy Res.* 6 (6), 515–530. doi:10.46690/ager.2022.06.08

Guo, Y., Wang, Y. C., Peng, J. S., Gao, K. S., Wu, Q. X., and Wu, H. M. (2018). Main controlling factors on the formation of high-quality reservoirs in the Middle and Lower Jurassic clastic rock buried hills in Qinan fault terrace belt,Bohai sea. *China Offshore Oil Gas* 30 (6), 41–50. doi:10.11935/j.issn.1673-1506.2018.06.005

Hou, M. C., Cao, H. Y., Li, H. Y., Chen, A. Q., Wei, A. J., Chen, Y., et al. (2015). Characteristics and controlling factors of deep buried-hill reservoirs in the BZ19-6 structural belt, Bohai Sea area. *Nat. Gas. Ind.* 39 (1), 33–44. doi:10.1016/j.ngib.2019.01.011

Hua, X. L., Li, H. Y., Sun, X. J., Tao, L., and Hu, H. W. (2020). Distribution pattern of high-quality reservoirs and karst zoning feature of carbonate rocks in buried hills: A case study from the bozhong sag, Bohai Bay Basin, China. *Acta pet. sin.* 26 (03), 333–338. doi:10.16108/j.issn1006-7493.2019059

Huang, S. B., Liu, L. F., Wu, K. Q., Chen, S. P., Jiang, X., and Hao, J. (2017). Control factors and comprehensive prediction of granite buried hill reservoirs in Western segment of Shaleitian bulge, Bohai Sea. *China pet. Explor.* 22 (4), 108–115. doi:10.3969/j.issn.1672-7703.2017.04.011

Jin, Z. K., Zou, Y. R., Jiang, C. L., and You, W. F. (2001). Distribution and controlli ng factors of ordovician karst reservoirs in Dagang region. *Acta sedimentol. sin.* 19 (4), 530–536. doi:10.14027/j.cnki.cjxb.2001.04.010

Li, H. Y., Xiao, S. G., Li, F., Liu, K., and Huang, Z. (2023). Reservoir characteristics and main controlling factors of hydrocarbon accumulation of lower paleozoic buried-hill in northwestern shaleitian slope of western Bohai Sea. *Earth Sci.* 48 (1), 329–341. doi:10.3799/dqkx.2022.406

Li, J. Y., Wang, Y. S., Liu, C. H., Dong, D. W., and Gao, Z. Q. (2016). Hydrothermal fluid activity and the quantitative evaluation of its impact on carbonate reservoirs: A case study of the lower paleozoic in the west of dongying sag, Bohai Bay Basin, east China. *Petroleum Explor. Dev.* 43 (03), 359–366. doi:10.1016/S1876-3804(16)30046-5

Li, W., Meng, M. F., Chen, X. P., Zhang, T. J., Yang, H. F., Niu, C. M., et al. (2021). Quantitative characterization of extension and compression derived from bending strike-slip faults and their petroleum geological significance of the eastern Bohai Sea. *J. China Univ. Petroleum(Edition Nat. Sci.* 45 (5), 23–32. doi:10.3969/j.issn.1673-5005.2021.05.003

Liu, C. F., Zhang, L., Li, Y. C., Liu, F. G., Martyushev, D. A., and Yang, Y. F. (2022). Effects of microfractures on permeability in carbonate rocks based on digital core technology. *Adv. Geo-Energy Res.* 6 (1), 86–90. doi:10.46690/ager.2022.01.07

Liu, J. S., Yang, H. M., Xu, K., Wang, Z. M., Liu, X. Y., Cui, L. J., et al. (2022). Genetic mechanism of transfer zones in rift basins: Insights from geomechanical models. *GSA Bull.* 134 (9-10), 2436–2452. doi:10.1130/b36151.1

Ma, L. C., Wang, Y. S., and Jing, A. Y. (2020). Discovery and significance of subtle buried hills in Jiyang depression, Bohai Bay Basin. *Petroleum Geol. Exp.* 042 (001), 13–18. doi:10.11781/sysydz202001013

Ni, X. F., Zhang, L. J., Shen, A. J., Qiao, Z. F., and Han, L. J. (2010). Diagenesis and pore evolution of the Ordovician karst reservoir in Yengimahalla-Hanilcatam region of Tarim baisn. *J. Palaeogeogr.* 12 (4), 467–480.

Tang, J. G., Hu, W. S., Li, W., and Zhang, G. Y. (2013). Prediction of weathering paleokarst reservoirs by combining paleokarst landform with unconformity: A case study of sinian dengying formation in Leshan–Longnüsi paleo-uplift, sichuan basin. *Petroleum Explor. Dev.* 40 (6), 722–730. doi:10.1016/s1876-3804(13)60097-x

Tang, L. J., Wan, G. M., Zhou, X. H., Jin, W. Z., and Yu, Y. X. (2008). Cenozoic geotectonic evolution of the Bohai basin. *Geol. J. China Univ.* 14 (2), 191–198. doi:10.16108/j.issn1006-7493.2008.02.001

Wang, X., Zhou, X. H., Xu, G. S., Liu, P. B., Gao, K. S., and Guan, D. Y. (2015). Characteristics and controlling factors of reservoirs in Penglai 9-1 large-scale oilfield in buried granite hills, Bohai Sea. *Oil gas Geol.* 36 (2), 262–270. doi:10.11743/ogg20150211

Wang, Y. C., Wei, A. J., Gao, K. S., Peng, J. S., Guo, Y., and Huang, Z. (2016). Development controlling factors and distribution predication of Ordovician carbonate reservoirs in northwestern part of Shaleitian arch, offshore Bohai Sea. *Mar. Orig. Pet. Geol.* 21 (02), 13–21. doi:10.3969/j.issn.1672-9854.2016.02.002

Wang, Y. S., and Li, J. Y. (2017). Characteristics and main controlling factors of layered reservoir in buried hill of carbonate rock in Pingfangwang Oilfield, Jiyang Depression. *J. China Univ. petroleum* 41 (04), 27–35. doi:10.3969/j.issn.1673-5005.2017.04.004

Wei, A. J. (2015). Characteristics, origin and quantitative evaluation of overpressure in strike-slip and compression-shear booster zone of Tan-Lu Fault:A case study in JZ27 section of Liaodong Bay, Bohai Sea. *Petroleum Geol. Exp.* 37 (1), 47–52. doi:10.11781/sysydz201501047

Xiao, Q., Ji, H. C., Liu, J. X., Guo, Q., Yang, F., Guo, J. Y., et al. (2018). Diagenesis and its effect to carbonate reservoirs of the Ordovician in Dongpu area. *J. Palaeogeogr.* 20 (02), 299–310. doi:10.7605/gdlxb.2018.02.022

Xie, Z. Y., Wei, G. Q., Li, J., Yang, W., Zhang, G. W., Guo, J. Y., et al. (2013). Reservoir characteristics and accumulation mode of large carbonate gasfields in China. *Acta pet. sin.* 034 (1), 29–40. doi:10.7623/syxb2013S1003

Xu, C. G., Hou, M. C., Wang, Y. C., Cheng, A. Q., Huang, Z. F., Luo, X. P., et al. (2019). Type and Genesis of Pre-Tertiary deep buried hills in the Bohai Sea area. *Nat. Gas. Ind.* 39 (01), 21–32. doi:10.3787/j.issn.1000-0976.2019.01.003

Ye, T., Chen, A. Q., Niu, C. M., Luo, J., and Hou, M. C. (2022a). Effective fractures linked with tectonic reactivation and multiple genetic fluids in the ultradeep Paleozoic carbonate buried hills of the Bozhong sag, North China. *Mar. petroleum Geol.* 140, 105642. doi:10.1016/j.marpetgeo.2022.105642

Ye, T., Niu, C. M., Wang, D. Y., Wang, Q. B., Dai, L. M., and Chen, A. Q. (2022b). Mesozoic tectonic evolution of the southwestern Bohai Sea and its dynamic mechanism: Implications for the destruction of the North China Craton. *Earth Sci. Front.* 29 (5), 133–146. doi:10.13745/j.esf.sf.2021.9.22

Ye, T., Wei, A. J., Gao, K. S., Sun, Z., and Li, F. (2020). New sequence division method of shallow platform with natural gamma spectrometry data: Implication for reservoir distribution—a case study from majiagou formation of bozhong 21–22 structure, Bohai Bay Basin. *Carbonate evaporates* 35, 116. doi:10.1007/s13146-020-00654-w

Yu, H. B., Wang, D. Y., Liu, C. M., and Li, L. (2015). Characteristics and formation mechanisms of buried hill carbonate reservoirs in Bonan Low Uplift, Bohai Bay. *Petroleum Geol. Exp.* 37 (02), 150–156. doi:10.7603/s40972-015-0024-4

Yu, Y. X., Zhou, X. H., Xu, C. G., Wu, K., Liu, Y. B., Yang, K. J., et al. (2014). Differential deformation of strike slip faults in the Liaodongwan depression, offshore Bohai Bay Basin. *Oil gas Geol.* 35 (5), 632–638. doi:10.11743/ogg20140507

Yun, L., and Deng, S. (2022). Structural styles of deep strike-slip faults in Tarim Basin and the characteristics of their control on reservoir formation and hydrocarbon accumulation:a case study of Shunbei oil and gas field. *Acta pet. sin.* 43 (6), 770–786. doi:10.7623/syxb202206003

Zhang, Q. L., Hou, G. T., Pan, W. Q., Han, J. F., Ju, Y., Li, L., et al. (2010). Development of fractures in carbonate rocks under the influence of strike-slip faults in Bachu area, Xinjiang, China. *Geol. Bull. China* 29 (8), 1160–1167.

Zhang, X. Q., Wu, Z. P., Zhou, X. H., Niu, C. M., Li, W., Ren, J., et al. (2017). Cenozoic tectonic characteristics and evolution of the southern Bohai Sea. *Geotect. metallogenia* 41 (1), 50–60. doi:10.16539/j.ddgzyckx.2017.01.004

Zhang, Y. D., Zhou, W., Deng, K., Wang, C. L., Wang, Y., and Meng, X. L. (2014). Palaeogeomorphology and reservoir distribution of the Ordovician karstified carbonate rocks in the structurally-gentle Gaoqiao area, Ordos Basin. *Acta petrol. sin.* 30 (3), 757–767.

Zhao, W. Z., Shen, A. J., Hu, S. Y., Zhang, B. M., Pan, W. Q., Zhou, J. G., et al. (2012). Geological conditions and distributional features of large-scale carbonate reservoirs onshore China. *Petroleum Explor. Dev.* 39 (01), 1–12. doi:10.1016/S1876-3804(12)60010-X

Zhao, W. Z., Shen, A. J., Pan, W. Q., Zhang, B. M., Zhang, G. W., Qiao, Z. F., et al. (2013). A research on carbonate karst reservoirs classification and its implication on hydrocarbon exploration: Cases studies from Tarim Basin. *Acta petrol. sin.* 29 (9), 3213–3235. doi:10.1086/671395

Zhao, X. Z., Wang, Q., Jin, F. M., Wang, H. C., Luo, J. Y., Zeng, J. H., et al. (2012). Reservoir characteristics and accumulation mode of large carbonate gasfields in China. *Acta pet. sin.* 33 (1), 71–79.

Zhou, X. H., Yu, Y. X., Tang, L. J., Lv, D. Y., and Wang, Y. B. (2010). Cenozoic offshore basin architecture and division of structural ele ments in Bohai sea. *China offshore oil gas* 22 (5), 285–289.

Zhu, X., Zhang, Q. L., and Hou, G. T. (2017). The controlling fator study of development of carbonatic roch fractures in the Kelpin-Bachu area, Xinjiang and its petroleum exploration significance. *Acta Geol. sin.* 91 (6), 118–1191.